minerals

MDPI

Article

Viscosity, Boson Peak and Elastic Moduli in the Na_2O-SiO_2 System

Michele Cassetta [1,2], Gino Mariotto [2], Nicola Daldosso [2], Emanuele De Bona [1], Mattia Biesuz [1], Gian Domenico Sorarù [1], Renat Almeev [3], Marco Zanatta [4] and Francesco Vetere [3,5,*]

[1] Department of Industrial Engineering, University of Trento, I-38122 Trento, Italy; emanuele.debona@unitn.it (E.D.B.)
[2] Department of Engineering for Innovation Medicine, University of Verona, I-37134 Verona, Italy
[3] Institut for Mineralogy, University of Hannover, D-30167 Hannover, Germany; r.almeev@mineralogie.uni-hannover.de
[4] Department Physics, University of Trento, I-38123 Trento, Italy
[5] Department of Physical Sciences, Earth and Environment, University of Siena, I-53100 Siena, Italy
* Correspondence: francesco.vetere@unisi.it

Abstract: The temperature and chemical dependence of the melt viscosity are ubiquitous in the model development of the volcanic dynamics, as well as in the glass production and design. We focussed on the yet-explored relationship between the bulk and shear moduli ratio and boson peak with the melt fragility of their parental glasses. Here, we explored the extension of the observed trend by testing the conventional binary system Na_2O-SiO_2, thus providing new evidence supporting the link between the flow of melts and supercooled liquids and the vibrational dynamics of their parental glasses. This was accomplished by integrating new low-frequency Raman measurements and integrating data from the literature on Brillouin light scattering and viscometry. This approach allows us to feed the MYEGA equation with reliable input parameters to quantitatively predict the viscosity of the Na_2O-SiO_2 system from the liquid up to the glass transition.

Keywords: viscosity; fragility; glass transition; boson peak; elastic moduli

Citation: Cassetta, M.; Mariotto, G.; Daldosso, N.; De Bona, E.; Biesuz, M.; Sorarù, G.D.; Almeev, R.; Zanatta, M.; Vetere, F. Viscosity, Boson Peak and Elastic Moduli in the Na_2O-SiO_2 System. *Minerals* **2023**, *13*, 1166. https://doi.org/10.3390/min13091166

Academic Editor: Yann Morizet

Received: 25 July 2023
Revised: 22 August 2023
Accepted: 30 August 2023
Published: 1 September 2023

1. Introduction

The shear viscosity η of glass-forming liquids is one of the central physical quantities for a vast set of disciplines ranging from geology to material science. Indeed, its temperature dependence controls the viscoelastic response of the material to deformations [1] and triggers several microscopic processes such as melt phase separation, bubbles clustering and crystals nucleation and growth. Broadly speaking, the viscosity influences the flow dynamics [2] and this represents one of the core issues of both volcanology [3,4] and glass design and production [5].

The dynamics, course and style of volcanic eruptions are strongly influenced by a complex interaction between physicochemical characteristics of magmas and processes occurring at different time and length scales [6,7]. Being magma multi-phase systems with a dominant liquid phase, the knowledge of viscosity is central in any modern modeling of volcanologically relevant processes [8,9]. Furthermore, the liquid viscosity range where supercooled liquids can be molded spans only a few orders of magnitude as compared to the huge increases of η from the liquid to the glass transition value. This impacts the qualities of melt workability and glass meltability which are, in turn, crucial properties for achieving a balance between the design and operation of glass melting and forming facilities. Actually, this has been known since the Middle Ages by Italian glassmakers who classified glass-former liquids as "lunghi" (long) and "corti" (fast) to distinguish the time needed to cross that region [10]. This ancient definition is currently effectively described by the fragility m. Consequently, a thorough study and microscopic modeling of the

temperature behavior of viscosity between the melting and the glass transition temperature is a substantial step toward "*better glasses*" [11].

The prototypical system $x$$Na_2O$-$-(1-x)SiO_2$ represents probably the most investigated proxy in material and geosciences. Experimental and theoretical studies cover both the liquid [12,13] and the glassy state [14,15]. Although widely different in composition from either natural or technological systems, this binary glass former potentially mimics most of the behavior of the soda–lime silicate systems and lava analogs of terrestrial and extraterrestrial volcanism [16–18]. Basically, the silica network is progressively depolymerized and compensated by the occurrence of non-bridging oxygens as the sodium concentration increases. In turn, the glass structure is softened and the glass transition temperature (T_g) is lowered [19]. Hence, the structure evolves, from a stressed rigid to a floppy structure [20]. This process significantly boosts the macroscopic dynamics of the system and directly governs the temperature T evolution of the viscosity as T_g is approached. This can be quantified by considering the fragility defined as:

$$m = \left.\frac{\partial \log_{10}\eta}{\partial T_g/T}\right|_{T=T_g} \quad (1)$$

This relation has been visualized for several systems in the well-known Angell's plot [21] where the different glass-forming liquids can be classified according to their fragility. In particular, "strong" or "fragile" melts show a quasi-/purely- or a non-Arrhenius dependence, respectively [21].

Several decades of work on sodium silicate glasses have produced a huge database of several physical properties, as well as a debate on the explanation of glass and melt properties [22,23]. Here, we add a further piece of information by providing a deepening of the T-dependence of the viscosity evolution as a function of the Na_2O concentration and its relation with the low-frequency (low-ω) region of the Raman spectra dominated by the so-called boson peak (BP). To do so, we exploit the same approach described by Cassetta et al., 2021 [24] and we focus on the correlation between m and the vibrational properties. The T behavior of the viscosity is obtained using the Mauro–Yue–Ellison–Gupta–Allan (MYEGA) equation [25]. Furthermore, the glass transition temperature of the high-silica endmember was measured and used to determine externally the predictions of the system using differential scanning calorimetry (DSC). Our results shed some new light on the mechanisms that lead to the evolution of viscoelastic properties in the supercooled liquid, providing a reference for future modeling of the macroscopic behavior of the glass-forming liquid.

2. Materials and Methods

We synthesized 5 binary sodium silicate glasses, by melting a binary mixture of SiO_2 and Na_2CO_3 powders (Sigma-Aldrich, St. Louis, MO, USA), after having milled together in agate mortar and mixed in bottles. The powders were melted in Pt-crucibles at 1780 K and quenched in air, thus experiencing the same cooling rate. The glass samples were annealed at their T_g for 2 h and cooled to ambient T at 10 K min^{-1}.

Samples are named using the prefix "NS", where N stands for soda (Na_2O), S for silica (SiO_2), whilst the number is the mol.% of Na_2O in the mixture, i.e., NS20 represents the mixture SiO_2 80 mol.%–Na_2O 20 mol.%.

The real density of the compounds was measured using He-pycnometry using an Ultrapyc5000 from Anton Paar®. All values reported in this work result from the average of 99 runs, performed at 20 °C in pulse mode (10 pulses) at the pressure of 10 psi.

The glass chemistry was determined at the Institute of Mineralogy, Leibniz University Hannover using an electron microprobe (JEOL JXA-iHP200F Field Emission Electron Probe Microanalyzer, Peabody, MA, USA). Compositions are summarized in Table S1 of the Supplementary Information (SI). Beam conditions on unknowns and calibration standards were 15 kV and 8 nA and defocused to 30 µm spot size. Si (Kα) and Na (Kα) were acquired

using TAP and TAPL crystals, respectively. At these conditions, well-known sodium loss (checked by Na counts for every 200 ms) was not observed within 10 s (checked for glasses). Measurement peak and background time were 10 and 5 s for SiO_2 and 5 and 2 s for Na_2O, respectively. Element calibrations were conducted using in-house basaltic glass standards whose compositions were verified against certified MPI-DING reference glasses [26]. Two additional Na_2O-rich albite and jadeite glasses were used as unknown references (in this case, Al_2O_3 was also included in measurements with conditions similar to those for SiO_2, 10 s/5 s, TAP(Kα)). Raman spectra were acquired with a micro-Raman spectrometer (Horiba Jobin-Yvon model T-64000, Villeneuve d'Ascq, France) having three holographic gratings (1800 lines/mm), configured in double subtractive/single mode, coupled with a CCD detector with 1024 × 256 pixels, and cooled by liquid nitrogen. Raman measurements were performed in backscattering geometry with the possibility of polarizing the laser beam for both parallel (HH) and crossed (HV) modes, which is provided by a combined Ar-Kr ion gas laser set at 514.5 nm (Spectra-Physics, Satellite 2018 RM, Mountain View, CA, USA). See refs. [27,28] for details.

A simultaneous thermogravimetric and DSC analyzer (TGA-DSC 3+, Mettler Toledo, Madison, WI, USA) was used to conduct the thermal analysis as described in refs. [29,30]. To remove the thermal history of the sample, a polished glass chip (about 10 mg) was put in an alumina crucible and heated from 300 to 1070 K at 20 K min^{-1} under air flowing at a rate of 100 mL min^{-1}. After cooling to ambient temperature at a rate of 10 K min^{-1}, the temperature was raised at the same rate to 1070 K. T_g was subsequently determined as the point where the tangent to the heat flow curve in the glassy state and that to the inflection point in the glass transition interval coincide.

Each glass was tested to be homogeneous at the microscopic scale by acquiring 20 HH Raman spectra in 20 different points using a 100× objective and checked to be consistent with the expected composition by comparing with those in the literature [31–33]. Spectra are reported in Figure S1 in the Supplementary Information (SI).

High- and low-temperature viscosity data were collected for the $xNa_2O - (1 - x)SiO_2$ from data from the literature: for NS15 from refs. [12,13,34,35] and ref. [22], data of samples B and C, for NS20 from refs. [12,13,22,34–36], for NS25 from refs. [12,13,35,37], for NS30 from refs. [13,35], for NS45 from ref. [35], and for sample NS10 we only collected low viscosity data from refs. [13,35]. The sound velocities of each composition were retrieved by interpolating the data from ref. [38]. The non-Arrhenius trends of each composition were fit to the MYEGA equation to the viscosity data from the literature and by setting $\eta_\infty = 10^{-2.93}$ Pa s, whilst the extrapolated values of m and T_g are reported in Table 1, as well as the longitudinal and transverse sound velocities v_l and v_t.

Table 1. Raman-derived boson peak position ω_{BP}, density measured using He-pycnometry ρ, glass transition temperature T_g, and fragility m obtained by fitting the viscosity data of the same composition found in the literature to the MYEGA equation. The longitudinal and transverse sound velocities v_l and v_t are reported together with the K/G. Data are from the references indicated in the last column. The uncertainties on the parameters are reported between brackets and is the error on the least significant digit of the result.

	ω_{BP}	ρ	T_g	m	v_l	v_t	K/G	Reference
	(cm^{-1})	(g cm^{-3})	(K)		(m s^{-1})	(m s^{-1})		
SiO_2	48.5(5)	2.20(2)	1427(8)	24.0(4)	5972	3769	1.18	[24]
NS10	49.7(6)	2.28(4)	-	-	5654	3531	1.23	(η) [13,34,35] (v_l, v_t)
NS15	51.0(1)	2.34(4)	779.9(5)	26.6(1)	5559	3421	1.31	(η) [12,13,34–36], (v_l, v_t) [37,38]
NS20	60.1(7)	2.39(2)	750.2(7)	29.8(2)	5493	3330	1.39	(η) [12,13,22,34–36], (v_l, v_t) [38]
NS25	60.0(7)	2.44(3)	731.0(1)	29.9(3)	5457	3257	1.47	(η) [12,13,35,37], (v_l, v_t) [38]
NS30	63.8(8)	2.47(2)	720.0(1)	30.8(2)	5450	3204	1.56	(η) [13,35], (v_l, v_t) [38]
NS45	71.0(1)	2.58(2)	679.7(5)	36.4(2)	5604	3154	1.82	(η) [35], (v_l, v_t) [38]

3. Results and Discussions

The glass densities (ρ) range from the typical value of silica glass (2.20 g cm^{-3}) to 2.58 g cm^{-3} for the sodic endmember NS45. Results are reported in Table 1, showing a good agreement with those of ref. [38]. Figure S1 shows the Raman spectra of the sample indicated in Table 1, which exhibit the peculiar band shape of SiO_2 and the sodium silicate glass systems [28,31,33,39,40]. Indeed, when sodium is added to the silica matrix, the R band dramatically decreases and a new band appears, namely the R_c band. It turns out relatively narrow and it gradually strengthens (both in frequency and intensity) as the sodium concentration increases. This extra band accompanying the R, D_1, and D_2 bands in alkali silicates is commonly detected even though its origin is still a matter of debate [39]. The low-ω region of the HV spectra Figure 1a–g is characterized by the strong appearance of the BP between 20 and 200 cm^{-1}. Below this spectral region, i.e., for frequencies $\omega \lesssim 20$ cm^{-1}, the spectrum generally shows an increase in intensity due to the quasi-elastic scattering (QES), which does not overlap with the BP, even if in silica-rich samples, is very shortly extended below the low-ω tail. Following these observations, in order to minimize the effect of the 460 cm^{-1} band superimposition [41,42], the whole evaluation of the BP is based on the HV spectra [43].

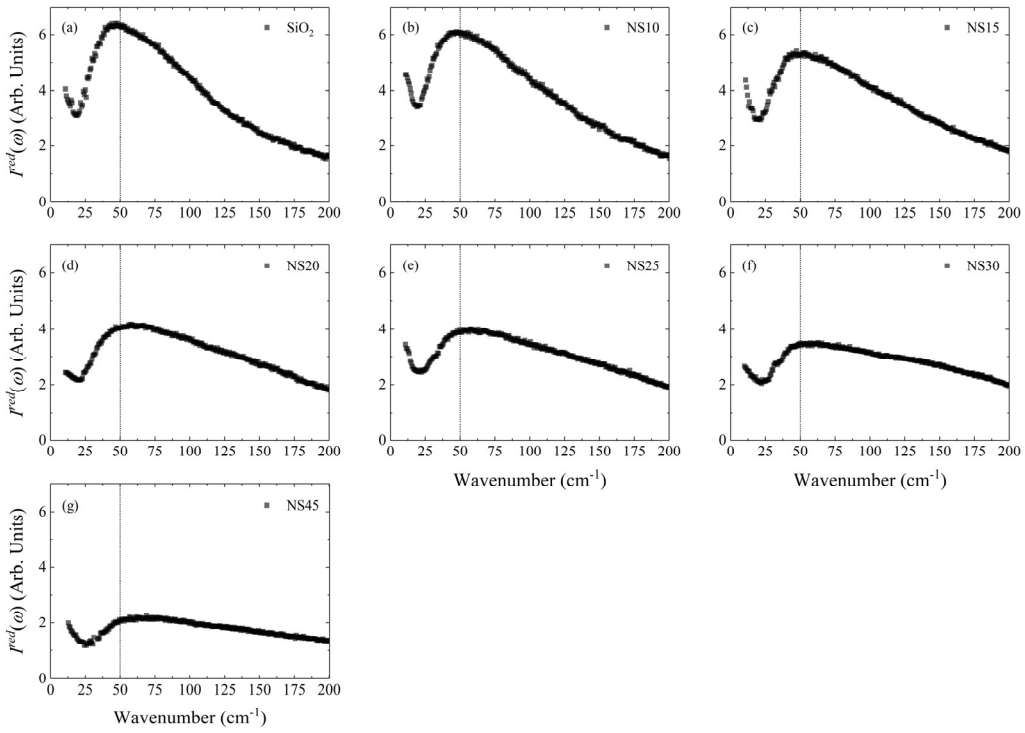

Figure 1. Reduced low-ω HV Raman spectra of binary sodium–silicate glasses (**a**–**g**). The red line is an example of the log-normal function defined as $I(\omega) \propto \exp\left\{-[\ln(\omega/\omega_{BP})]^2/2\sigma^2\right\}$, used for the fitting procedure. Here, σ is the width of the BP.

In a Raman scattering experiment on a glass [44], the scattered light depends on the vibrational density of states (VDOS) $g(\omega)$ through a coupling between photons and vibrations, effectively considered with the light-vibration coupling function $C(\omega)$. Thus, for a first-order Raman scattering experiment, the Stokes experimental intensity I^{obs} can be written as:

$$I^{obs}(\omega) = C(\omega)g(\omega)\frac{[n(\omega,T)+1]}{\omega} \quad (2)$$

where $n(\omega,T) = [\exp(\hbar\omega/k_BT) - 1]^{-1}$ is the Bose–Einstein population factor, k_B and $\hbar$ are the Boltzmann and the reduced Planck constants, respectively. Dividing the Raman

intensity by $[n(\omega,T) + 1]$ and ω, we obtain the reduced Raman intensity $I^{red}(\omega)$, which is proportional to the reduced density of vibrational states $g(\omega)/\omega^2$:

$$I^{red}(\omega) = C(\omega)\frac{g(\omega)}{\omega^2} \quad (3)$$

Thus, the peak of $I^{red}(\omega)$ is essentially the peak in $g(\omega)/\omega^2$ unlike in $C(\omega)$ which is assumed to be $C(\omega) \sim \omega$, and thus found to depend approximately linearly on frequency in the region of the BP, for a wide number of glasses [45–47]. The result of the treatment is reported in Figure 1. The parameters of the BP and in particular its maximum is usually obtained using a fit with a log-normal function, as proposed by Malinovsky and co-workers [48]. Consequently, we consider the BP position ω_{BP} defined as the maximum position in the reduced intensity, with an uncertainty of ~1 cm^{-1}.

Figure 1a reports the boson peak of SiO_2 glass plotted in the reduced intensity and fitted to the log-normal (red curve). The ω_{BP} shift to higher frequencies as the Na_2O concentration increases but once the system reaches ~20% of Na_2O the trend drops to form a step-like shape. It is worth keeping in mind that within this chemical interval often occurs the well-documented process called phase separation in the long-range order structural domain of the supercooled liquid [49]. This process results in a heterogeneous matrix in which different nano-sized regions having different concentrations (probably due to segregation [50,51]), originate nano-domains with different elastic constants, which may deeply influence the general behavior of the elastic medium properties. Indeed, the sharp reduction of T_g mirrors a heavy alteration of the mechanical equilibrium that prevailed [52] in the pristine glass (pure and slightly Na-doped silica) and drives mixed glasses to become stressed and rigid. This is largely the case because the bond-bending constraint of bridging oxygen atoms that were intrinsically broken [53] at ~1450 K becomes restored in the weakly alloyed glass as T_g dramatically drops to ~700 K. However, upon continuous addition of Na_2O, the glass softens as network connectivity decreases, and one expects an elastic phase transition from a stressed rigid phase to a floppy one. As a matter of fact, this behavior is mirrored by the chemically driven trends of sound velocities and elastic modulus that generally deviate from linearity from ~20% of Na_2O from both experiments [38] and molecular dynamics simulations [54]. At this point, the network of this system is defined as *isostatic*, which is free of internal modes of deformation and stresses. When compared with the trend observed in ref. [24], the overall distribution, although scattered, confirms the inverse correlation between ω_{BP} and SiO_2 content; Figure 2a. The correlation observed so far follows the conclusions outlined by ref. [55], in which the ω_{BP} shift to higher frequencies as the mean atomic volume, V_M, decreases, thus mirroring the interatomic distance. Our results are in line with the analysis and results of the low-ω Raman spectroscopy (in NS20 and NS30 compositions) presented in ref. [56] and with those retrieved by the low-temperature heat capacity of alkali silicate glasses described in ref. [57]. Our results are also reasonably similar to those of ref. [55] for composition NS10 and NS20 (differing just for a few cm^{-1}) whilst for higher Na_2O content, our results deviate by several cm^{-1}, displaying however values much closer to those found in ref. [31]. Generally, our results and those of the literature (although slightly in disagreement) agree unanimously that the addition of sodium reduces the BP intensity, which is higher for more polymerized structures. This trend can be observed in the $I^{red}(\omega)$ plot of Figure 1 highlighting the difference of magnitude from pure SiO_2 to NS45.

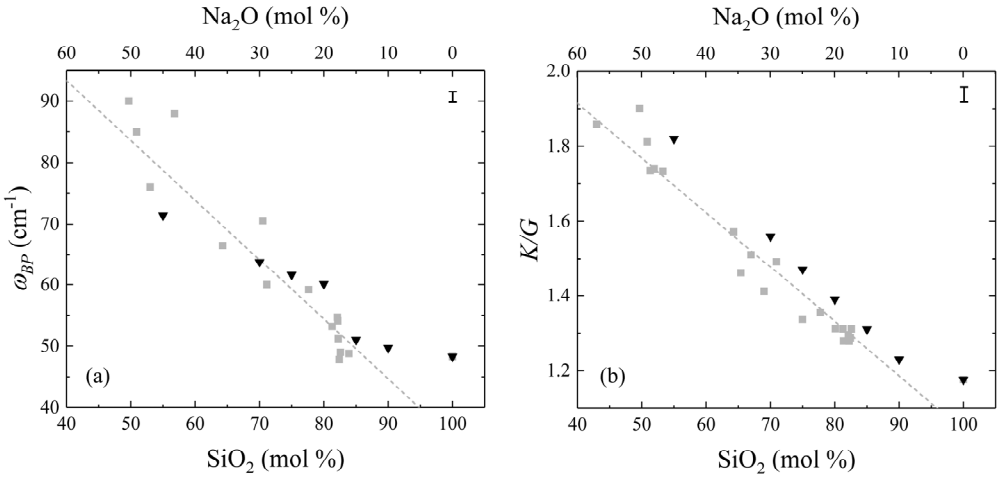

Figure 2. Boson peak (**a**) and K/G ratio (**b**) of samples from this study (black triangles) and those from ref. [24] (grey squares) as a function of the SiO_2 (mol%) content of the glasses. The dashed grey lines are the same linear fits from ref. [24] such as $\omega_{BP} = -1.0 \cdot SiO_2 + 133$ and $K/G = -0.0146 \cdot SiO_2 + 2.50$. The black bars on the upper right corner of the panels represent the largest extension of the error.

Conversely, the K/G in function of SiO_2 turns out linear and slightly shifted from the trend observed in ref. [24]; Figure 2b.

The ability to determine melt viscosity from the spectroscopic analysis of their parental glasses first depends on the determination of a correlation between the melt fragility m and glass transition temperature T_g with at least the ratio of the bulk and shear moduli K/G and BP. These later can be derived using Raman or Brillouin spectroscopy, whilst T_g can be measured by DSC and adopting the condition described in ref. [24] with proper shift factors. The relaxed liquid is firstly cooled into the supercooled region at 10 K min^{-1}, then a same-speed heating scan will mark de facto the T_g identified as the onset of the phase transition from glass to supercooled liquid.

Black squares in Figure 3a show data from this work that display a correlation between the fragility and BP position, in which ω_{BP} shift to higher frequencies as m increases, thus finding a general agreement with that found in ref. [24] (grey squares). Although linear in a short m interval, it keeps an exponential form that seems to match the asymptotic trend at m = 14.97, *the minimum* possible value within the MYEGA formulation [58]. Conversely, data derived via sound velocities (expressed by the K/G ratio, black squares), seems to line up through another pattern with a lower slope with respect to those found in ref. [24] (grey squares), see Figure 3b. This behavior indicates that this series looks shifted towards the relation proposed by Novikov and Sokolov [59], revealing probably that the macroscopic elastic properties of this binary system deviate substantially from those of multicomponent ones (i.e., involving different species of glass formers or intermediates Al_2O_3 or Fe_2O_3).

Figure 4 shows the predicted viscosity of our binary system calculated through the MYEGA equation vs. the measured viscosity data collected from the literature, for a total of 200 viscosity data. The temperature dependence of η was obtained by replacing m derived by the model of ref. [24] and the T_g reported in Table 1 and then setting the $\eta_\infty = 10^{-2.93}$ Pa s. The resulting root-mean-square error (RMSE) for this investigated binary series is 0.03 for Raman and 0.13 for Brillouin. This test shows that a further external validation produces RMSE values lower than those of ref. [24]; thus, the accuracy is significantly below the estimated error, especially for Raman. Both approaches accurately corroborate the literature on current data.

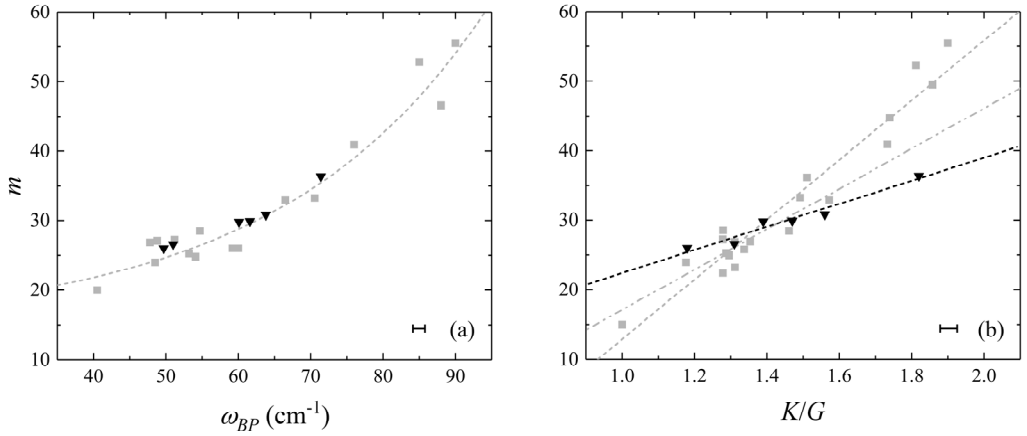

Figure 3. Relationship between the melt fragility m and spectroscopic parameters (black triangles) boson peak position ω_{BP} in (**a**) and the ratio between bulk and shear modulus K/G in (**b**). The black bars represent the largest extension of the error. Dashed grey lines are the fits of [24], $m = 1.7 \exp(\omega_{BP}/28) + 14.97$ in (**a**) and $m = 43 \cdot K/G - 31$ in (**b**), whilst the grey dash–dot–dot line in (**b**) reports the correlation found by Novikov and Sokolov [59] $m = 29 \cdot (K/G - 0.41)$. The black dashed fit is calculated only for the studied binary series (excluding SiO_2) for comparison. Grey squares are data from ref. [24].

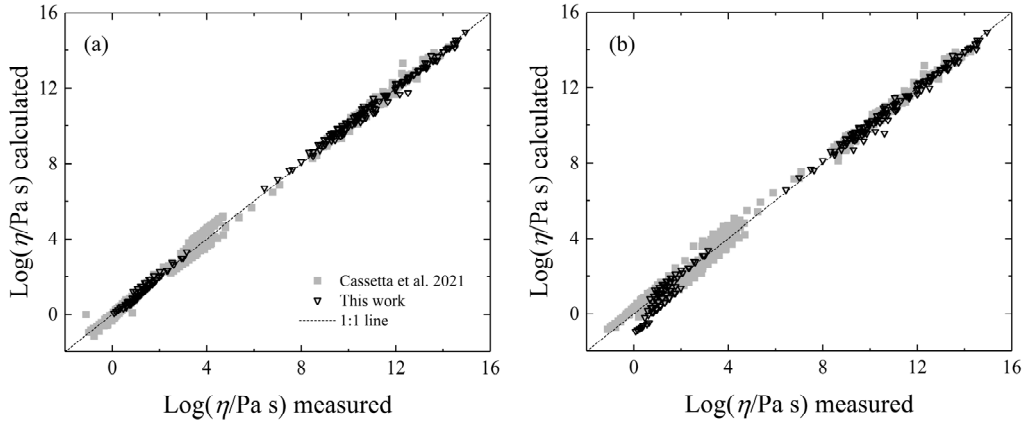

Figure 4. Comparison between the measured viscosity data from the literature and the viscosities predicted using the model of Cassetta et al. (see ref. [24]) with m derived by $m(\omega_{BP})$ (**a**) and $m(K/G)$ (**b**). Grey squares are predicted vs. measured viscosity data from ref. [24].

Finally, we use an external sample whose low-viscosity data are missing in the literature to validate our assumptions by measuring its glass transition temperature. The relaxed liquid is first cooled into the supercooled area at 10 K min^{-1}, and the subsequent DSC heating scan is then carried out at the same rate. This treatment provided the T_g of the sample (774 ± 1 K) which corresponds to $\eta = 10^{12}$ Pa s. Figure 5a shows the heat flow as a function of temperature for the NS10 glass sample (90% mol SiO_2) where the grey dashed lines indicate the tangents defining the onset of the glass transition (T_g). Figure 5b shows the measured viscosity from the literature [13,35] with Raman- and Brillouin-based estimates using the BP position and the K/G ratio, respectively. Our data show that the methodology followed offers precise low- and high-temperature viscosity projection (lines). A close look at the model shows that the BP-based prediction slightly underestimates the high-T viscosity unlike the K/G-based model, which overestimates with a comparable magnitude. Moreover, we want to emphasize that the cooling rates applied to the glasses on which the model of study [24] was conducted were essentially unknown and varied. Yet, the effectiveness of our validation shows that, also within this binary system, typical laboratory cooling rates do not appreciably impact the link between K/G and BP of the

glasses and melt fragility m of their parental melts. This implication is supported by the findings of refs. [60,61] revealing no distinction between quenched and annealed glasses in the ω_{BP} and in the elastic parameters, thus demonstrating the lack of a significant link to the extended structure of binary silicate glasses.

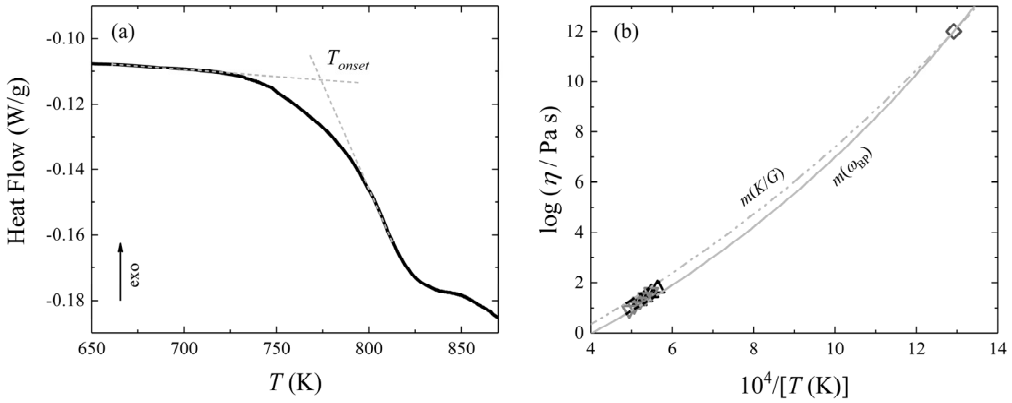

Figure 5. (**a**) Heat flow as a function of temperature of the NS10 glass (90% mol SiO_2). Grey dashed lines represent the tangents defining the onset of the glass transition (T_{onset}). (**b**) External prediction of the NS10 melt viscosity. Symbols represent measured viscosity data: triangles from the literature (grey triangles from ref. [13] and black triangles from ref. [35]) and square is $\eta(T_g) = 10^{12}$ Pa s.

4. Conclusions

The Raman and Brillouin data confirm again that the melt fragility can be retrieved by spectroscopic parameters embedded in glasses. Additionally, a valid estimation of viscosity can be extended to this straightforward binary system by integrating the T_g into the MYEGA equation. Our results are predicted by the model [24] with significantly lower RMSE (by 90% for Raman and 46% for Brillouin). We additionally observed that new measurements and the exhaustive examination of the literature both point to a clear connection between BP and the acoustic modes. Beyond the predictions discussed in the literature, we report here a direct relationship between the ratio of the bulk and shear moduli and the BP position (ω_{BP}). We thus take advantage of the ongoing discussion surrounding the BP phenomenon to present fresh data that may contribute to a better understanding of its theoretical description.

Supplementary Materials: The following supporting information can be downloaded at: https://www.mdpi.com/article/10.3390/min13091166/s1, Figure S1: HH Raman spectra; Table S1: EMPA determinations and densities.

Author Contributions: Conceptualization, M.C., F.V. and M.Z.; methodology, M.C., G.M., E.D.B., M.B. and R.A.; validation, M.C., M.Z. and F.V.; formal analysis, M.C., R.A. and E.D.B.; investigation, M.C.; resources, F.V., G.M., N.D., M.B. and G.D.S.; data curation, M.C.; writing—original draft preparation, M.C.; writing—review and editing, F.V., M.Z., M.B., E.D.B., R.A., N.D., G.M. and G.D.S.; visualization, M.C.; supervision, M.Z. and F.V.; project administration, M.C.; funding acquisition, G.M., M.B. and G.D.S. All authors have read and agreed to the published version of the manuscript.

Funding: F. Vetere acknowledges the "Piano di Sostegno alla Ricerca 2022 per finanziamenti a progetti di ricerca Curiosity-driven (F-CUR) Cinetiche di cRistallizzazionE nei mAgMI–CREAMI 2263-2022-VF-CONRICMIUR_PC-FCUR_002". This work was also funded by the European Office of Aerospace Research and Development (U.S. Air Force Office of Scientific Research) within the project "From polymers to covalent glasses (PolGla)", Award Nr. FA8655-23-1-724.

Acknowledgments: All authors acknowledge B. Giannetta and C. Zaccone for the DSC measurements.

Conflicts of Interest: The authors declare no conflict of interest.

References

1. Maxwell, J.C. On the Dynamical Theory of Gases. *Philos. Trans. R. Soc. Lond.* **1867**, *157*, 49–88.
2. Zanotto, E.D.; Cassar, D.R. The race within supercooled liquids—Relaxation versus crystallization. *J. Chem. Phys.* **2018**, *149*, 2. [CrossRef]
3. Gonnermann, H.M.; Manga, M. The Fluid Mechanics Inside a Volcano. *Annu. Rev. Fluid Mech.* **2007**, *39*, 321–356. [CrossRef]
4. Dingwell, D.B. Volcanic dilemma: Flow or blow? *Science* **1996**, *273*, 1054–1055. [CrossRef]
5. Zanotto, E.D.; Mauro, J.C. The glassy state of matter: Its definition and ultimate fate. *J. Non-Cryst. Solids* **2017**, *471*, 490–495. [CrossRef]
6. Vetere, F.; Iezzi, G.; Behrens, H.; Holtz, F.; Ventura, G.; Misiti, V.; Cavallo, A.; Mollo, S.; Dietrich, M. Glass forming ability and crystallisation behaviour of sub-alkaline silicate melts. *Earth-Sci. Rev.* **2015**, *150*, 25–44. [CrossRef]
7. Di Genova, D.; Brooker, R.A.; Mader, H.; Drewitt, J.W.E.; Longo, A.; Deubener, J.; Neuville, D.R.; Fanara, S.; Shebanova, O.; Anzellini, S.; et al. In situ observation of nanolite growth in volcanic melt: A driving force for explosive eruptions. *Sci. Adv.* **2020**, *6*, eabb0413. [CrossRef]
8. Giordano, D.; Russel, J.K.; Dingwell, D.B. Viscosity of magmatic liquids: A model. *Earth Planet. Sci. Lett.* **2008**, *271*, 123–134. [CrossRef]
9. Vetere, F.; Holtz, F. Rheological Behavior of Partly Crystallized Silicate Melts under Variable Shear Rate. *Dyn. Magma Evol. Geophys. Monogr.* **2021**, *1*, 152–167.
10. Scopigno, T. *La Transizione Vetrosa*; KOS: Milano, Italy, 2005; pp. 28–31.
11. Anderson, P.W. The deepest and most interesting unsolved problem in solid state theory. *Science* **1995**, *267*, 1615–1616. [CrossRef]
12. Poole, J.P. Low-Temperature Viscosity of Alkali Silicate Glasses. *J. Am. Ceram. Soc.* **1949**, *32*, 230–233. [CrossRef]
13. Bockris, J.O.; Lowe, D.C. Viscosity and the structure of molten silicates. *Proc. R. Soc.* **1954**, *226*, 423–435.
14. Hannon, A.C.; Vaishnav, S.; Alderman, O.L.G.; Bingham, P.A. The structure of sodium silicate glass from neutron diffraction and modeling of oxygen- oxygen correlations. *J. Am. Ceram. Soc.* **2021**, *104*, 6155–6171. [CrossRef]
15. Inoue, K.; Kataoka, H.; Nagai, Y.; Hasegawa, M.; Kobayashi, Y. Short and medium range order in two-component silica glasses by positron annihilation spectroscopy. *J. Appl. Phys.* **2014**, *115*, 20. [CrossRef]
16. Deubener, J.; Behrens, H.; Müller, R. An overview on the effect of dissolved water on the viscosity of soda lime silicate melts. *J. Non-Cryst. Solids* **2023**, *19*, 100195. [CrossRef]
17. Vetere, F.; Rossi, S.; Namur, O.; Morgavi, D.; Misiti, V.; Mancinelli, P.; Petrelli, M.; Pauselli, C.; Perugini, D. Experimental constraints on the rheology, eruption, and emplacement dynamics of analog lavas comparable to Mercury's northern volcanic plains. *J. Geophys. Res. Planets* **2017**, *122*, 1522–1538. [CrossRef]
18. Richet, P. Viscosity and configurational entropy of silicate melts. *Geochim. Cosmochim. ACTA* **1984**, *48*, 471–483. [CrossRef]
19. Greaves, G.N.; Sen, S. Inorganic glasses, glass-forming liquids and amorphizing solids. *Adv. Phys.* **2007**, *56*, 1–166. [CrossRef]
20. Micoulaut, M. Constrained interactions, rigidity, adaptative networks, and their role for the description of silicates. *Am. Mineral.* **2008**, *93*, 1732–1748. [CrossRef]
21. Angell, C.A. Formation of glasses from liquids and biopolymers. *Science* **1995**, *267*, 1924–1935. [CrossRef]
22. Jarry, P.; Richet, P. Unmixing in sodium-silicate melts: Influence on viscosity and heat capacity. *J. Non-Cryst. Solids* **2001**, *293–295*, 232–237. [CrossRef]
23. Le Losq, C.; Neuville, D.R. Molecular structure, configurational entropy and viscosity of silicate melts: Link through the Adam and Gibbs theory of viscous flow. *J. Non-Cryst. Solids* **2017**, *463*, 175–188. [CrossRef]
24. Cassetta, M.; Di Genova, D.; Zanatta, M.; Ballaran, T.B.; Kurnosov, A.; Giarola, M.; Mariotto, G. Estimating the viscosity of volcanic melts from the vibrational properties of their parental glasses. *Sci. Rep.* **2021**, *11*, 13072. [CrossRef] [PubMed]
25. Mauro, J.C.; Yue, Y.; Ellison, A.J.; Gupta, P.K.; Allan, D.C. Viscosity of glass-forming liquids. *Proc. Natl. Acad. Sci. USA* **2009**, *106*, 19780–19784. [CrossRef] [PubMed]
26. Jochum, K.P.; Stoll, B.; Herwig, K.; Willbold, M.; Hofmiann, A.W.; Amini, M.; Aarburg, S.; Abouchami, W.; Hellebrand, E.; Mocek, B.; et al. MPI-DING reference glasses for in situ microanalysis: New reference values for element concentrations and isotope ratios. *Geochem. Geophys. Geosyst.* **2006**, *7*, 2. [CrossRef]
27. Cassetta, M.; Zanatta, M.; Biesuz, M.; Giarola, M.; Mariotto, G. New insights about the role of Na–K ratio on the vibrational dynamics of synthetic-basalt glasses. *J. Raman Spectrosc.* **2022**, *53*, 540–549. [CrossRef]
28. Enrichi, F.; Cassetta, M.; Daldosso, N.; Cattaruzza, E.; Riello, P.; Zairov, R.; Vomiero, A.; Righini, G.C. Effect of the crystal structure on the optical properties and Ag sensitization of Tb^{3+}/Yb^{3+} ions in silica-zirconia glasses and glass-ceramics. *Ceram. Int.* 2022, *in press*. [CrossRef]
29. Cassetta, M.; Giannetta, B.; Enrichi, F.; Zaccone, C.; Mariotto, G.; Giarola, M.; Nodari, L.; Zanatta, M.; Daldosso, N. Effect of the alkali vs iron ratio on glass transition temperature and vibrational properties of synthetic basalt-like glasses. *Spectrochim. Acta Part A Mol. Biomol. Spectrosc.* **2023**, *293*, 122430. [CrossRef]
30. Cassetta, M.; Vetere, F.; Zanatta, M.; Perugini, D.; Alvaro, M.; Giannetta, B.; Zaccone, C.; Daldosso, N. Micro-Raman spectroscopy for a comprehensive understanding of the structural evolution of Basaltic-Andesite and Trachybasalt multiphase systems. *Chem. Geol.* **2023**, *616*, 121241. [CrossRef]

31. Furukawa, T.; Fox, K.E.; White, W.B. Raman spectroscopic investigation of the structure of silicate glasses. III. Raman intensities and structural units in sodium silicate glasses. *J. Chem. Phys.* **1981**, *75*, 3226–3237. [CrossRef]
32. O'Shaughnessy, C.; Henderson, G.S.; Nesbitt, H.W.; Bancroft, G.M.; Neuville, D.R. The influence of modifier cations on the Raman stretching modes of Q_n species in alkali silicate glasses. *J. Am. Ceram. Soc.* **2020**, *103*, 3991–4001. [CrossRef]
33. Malfait, W.J.; Zakaznova-Herzog, V.P.; Halter, W.E. Quantitative Raman spectroscopy: Speciation of Na-silicate glasses and melts. *Am. Mineral.* **2008**, *93*, 1505–1518. [CrossRef]
34. Mazurin, O.V.; Streltsina, M.V.; Shvaiko-Svaikovskaya, T.P. *Handbook of Glass Data Part A: Silica Glass and Binary Silicate Glasses, A*; Elsevier: Amsterdam, The Netherlands, 1983.
35. Knoche, R.; Dingwell, D.B.; Seifert, F.A.; Webb, S.L. Non-linear properties of supercooled liquids in the system Na_2OSiO_2. *Chem. Geol.* **1994**, *116*, 1–16. [CrossRef]
36. Sipp, A.; Bottinga, Y.; Richet, P. New high viscosity data for 3D network liquids and new correlations between old parameters. *J. Non-Cryst. Solids* **2001**, *288*, 166–174. [CrossRef]
37. Le Losq, C.; Neuville, D.R.; Florian, P.; Henderson, G.S.; Massiot, D. The role of Al^{3+} on rheology and structural changes in sodium silicate and aluminosilicate glasses and melts. *Geochim. Cosmochim. Acta* **2014**, *126*, 495–517. [CrossRef]
38. Vaills, Y.; Luspin, Y.; Hauret, G. Two opposite effects of sodium on elastic constants of silicate binary glasses. *Mater. Sci. Eng. B* **1996**, *40*, 199–202. [CrossRef]
39. Hehlen, B.; Neuville, D.R.; Kilymis, D.; Ispas, S. Bimodal distribution of Si–O–Si angles in sodo-silicate glasses. *J. Non-Cryst. Solids* **2017**, *469*, 39–44. [CrossRef]
40. Zhao, Q.; Guerette, M.; Huang, L. Nanoindentation and Brillouin light scattering studies of elastic moduli of sodium silicate glasses. *J. Non-Cryst. Solids* **2012**, *358*, 652–657. [CrossRef]
41. Galeener, F.L. Band limits and the vibrational spectra of tetrahedral glasses. *Phys. Rev. B* **1979**, *19*, 4292–4297. [CrossRef]
42. Wang, Z.; Cooney, T.F.; Sharma, S.K. High temperature structural investigation of $Na_2O{\cdot}0.5Fe_2O_3{\cdot}3SiO_2$ and $Na_2O{\cdot}FeO_3$ SiO_2 melts and glasses. *Contrib. Mineral. Petrol.* **1993**, *115*, 112–122. [CrossRef]
43. Hehlen, B.; Simon, G. The vibrations of vitreous silica observed in hyper-Raman scattering. *J. Raman Spectrosc.* **2012**, *43*, 1941–1950. [CrossRef]
44. Baldi, G.; Fontana, A.; Monaco, G.; Orsingher, L.; Rols, S.; Rossi, F.; Ruta, B. Connection between Boson Peak and Elastic Properties in Silicate Glasses. *Phys. Rev. Lett.* **2009**, *102*, 195502. [CrossRef] [PubMed]
45. Fontana, A.; Dell'Anna, R.; Montagna, M.; Rossi, F.; Viliani, G.; Ruocco, G.; Sampoli, M.; Buchenau, U.; Wischnewski, A. The Raman coupling function in amorphous silica and the nature of the long-wavelength excitations in disordered systems. *Europhys. Lett.* **1999**, *47*, 56–62. [CrossRef]
46. Fontana, A.; Rossi, F.; Viliani, G.; Caponi, S.; Fabiani, E.; Baldi, G.; Ruocco, G.; Maschio, R.D. The Raman coupling function in disordered solids: A light and neutron scattering study on glasses of different fragility. *J. Phys. Condens. Matter.* **2007**, *19*, 205145. [CrossRef]
47. Surovtsev, N.V.; Sokolov, A.P. Frequency behavior of raman coupling coefficient in glasses. *Phys. Rev. B Condens. Matter Mater. Phys.* **2002**, *66*, 054205. [CrossRef]
48. Malinovsky, V.K.; Novikov, V.N.; Sokolov, A.P. Log-normal spectrum of low-energy vibrational excitations in glasses. *Phys. Lett. A* **1991**, *153*, 63–66. [CrossRef]
49. Weinberg, M.C.; Neilson, G.F. Phase separation behaviour of a metal-organic derived sodium silicate glass. *J. Mater. Sci.* **1978**, *13*, 1206–1216. [CrossRef]
50. Chen, P.; Holbrook, C.; Boolchand, P.; Georgiev, D.G.; Jackson, K.A.; Micoulaut, M. Intermediate phase, network demixing, boson and floppy modes, and compositional trends in glass transition temperatures of binary As_xS_{1-x} system. *Phys. Rev. B Condens. Matter Mater. Phys.* **2008**, *78*, 224208. [CrossRef]
51. Le Losq, C.; Neuville, D.R.; Chen, W.; Florian, P.; Massiot, D.; Zhou, Z.; Greaves, G.N. Percolation channels: A universal idea to describe the atomic structure and dynamics of glasses and melts. *Sci. Rep.* **2017**, *7*, 16490. [CrossRef]
52. Bauchy, M. Topological Constraint Theory and Rigidity of Glasses. *arXiv* **2020**, arXiv:2005.04603.
53. Bauchy, M.; Micoulaut, M. Atomic scale foundation of temperature-dependent bonding constraints in network glasses and liquids. *J. Non-Cryst. Solids* **2011**, *357*, 2530–2537. [CrossRef]
54. Jabraoui, H.; Vaills, Y.; Hasnaoui, A.; Badawi, M.; Ouaskit, S. Effect of sodium oxide modifier on structural and elastic properties of silicate glass. *J. Phys. Chem. B* **2016**, *120*, 13193–13205. [CrossRef]
55. Nakamura, K.; Takahashi, Y.; Osada, M.; Fujiwara, T. Low-frequency Raman scattering in binary silicate glass: Boson peak frequency and its general expression. *J. Ceram. Soc. Jpn.* **2013**, *121*, 1012–1014. [CrossRef]
56. Chemarin, C.; Champagnon, B. Medium range order in sodium silicate glasses: Role of the network modifier. *J. Non-Cryst. Solids* **1999**, *243*, 281–284. [CrossRef]
57. Richet, N.F. Heat capacity and low-frequency vibrational density of states. Inferences for the boson peak of silica and alkali silicate glasses. *Phys. B Condens. Matter.* **2009**, *404*, 3799–3806. [CrossRef]
58. Zheng, Q.; Zheng, J.; Solvang, M.; Yue, Y.; Mauro, J.C. Determining the liquidus viscosity of glass-forming liquids through differential scanning calorimetry. *J. Am. Ceram. Soc.* **2020**, *103*, 6070–6074. [CrossRef]
59. Novikov, V.N.; Sokolov, A.P. Poisson's ratio and the fragility of glass-forming liquids. *Nature* **2004**, *431*, 961–963. [CrossRef]

60. McIntosh, C.; Toulouse, J.; Tick, P. The Boson peak in alkali silicate glasses. *J. Non-Cryst. Solids* **1997**, *222*, 335–341. [CrossRef]
61. Whittington, A.G.; Richet, P.; Polian, A. Amorphous materials: Properties, structure, and durability: Water and the compressibility of silicate glasses: A Brillouin spectroscopic study. *Am. Mineral.* **2012**, *97*, 455–467. [CrossRef]